ACS Energy LETTERS

http://pubs.acs.org/journal/aelccp

LETTER

Zn–Se–Cd–S Interlayer Formation at the CdS/$Cu_2ZnSnSe_4$ Thin-Film Solar Cell Interface

Marcus Bär,[*,#,○] Ingrid Repins,[§] Lothar Weinhardt,[∥,†,⊥] Jan-Hendrik Alsmeier,[#] Sujitra Pookpanratana,[†,▽] Monika Blum,[†] Wanli Yang,[‡] Clemens Heske,[∥,†,⊥] Regan G. Wilks,[#] and Rommel Noufi[§]

[#]Renewable Energy, Helmholtz-Zentrum Berlin für Materialien und Energie GmbH (HZB), Berlin, Germany

[○]Institut für Physik, Brandenburgische Technische Universität Cottbus-Senftenberg, Cottbus, Germany

[§]National Renewable Energy Laboratory (NREL), Golden, Colorado, United States

[∥]Institute for Photon Science and Synchrotron Radiation (IPS), Karlsruhe Institute of Technology (KIT), Eggenstein-Leopoldshafen, Germany

[†]Department of Chemistry and Biochemistry, University of Nevada, Las Vegas (UNLV), Las Vegas, Nevada, United States

[⊥]Institute for Chemical Technology and Polymer Chemistry (ITCP), Karlsruhe Institute of Technology (KIT), Karlsruhe, Germany

[▽]Engineering Physics Division, National Institute of Standards and Technology, Gaithersburg, Maryland, United States

[‡]Advanced Light Source (ALS), Lawrence Berkeley National Laboratory, Berkeley, California, United States

ABSTRACT: **The chemical structure of the CdS/$Cu_2ZnSnSe_4$ (CZTSe) interface was studied by a combination of electron and X-ray spectroscopies with varying surface sensitivity. We find the CdS chemical bath deposition causes a "redistribution" of elements in the proximity of the CdS/CZTSe interface. In detail, our data suggest that Zn and Se from the Zn-terminated CZTSe absorber and Cd and S from the buffer layer form a Zn–Se–Cd–S interlayer. We find direct indications for the presence of Cd–S, Cd–Se, and Cd–Se–Zn bonds at the buffer/absorber interface. Thus, we propose the formation of a mixed Cd(S,Se)–(Cd,Zn)Se interlayer. We suggest the underlying chemical mechanism is an ion exchange mediated by the amine complexes present in the chemical bath.**

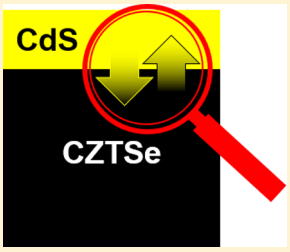

Thin-film solar cell absorbers based on the earth-abundant $Cu_2ZnSn(S,Se)_4$ (CZTSSe) kesterite material system have attracted much attention in the recent past, and the efficiency of respective devices has increased correspondingly. On a lab scale, kesterite-based solar cells already yield efficiencies up to 12.6%.[1] This progress is quite remarkable, as kesterite-based devices use a heterostructure cell design that was developed and optimized for a different material or device class, namely for *chalcopyrite*-based (Cu(In,Ga)Se_2, "CIGSe") devices. In this cell design, the front contact is usually formed by consecutive chemical bath deposition (CBD) of a CdS (buffer) layer and sputter-deposition of a transparent ZnO layer. To support further performance improvement of the *kesterite* system, e.g., by deliberate tailoring of interface properties, detailed insight into the chemical structure of status-quo kesterite devices and their interfaces is necessary.

In the past, the chemical structure of the CdS/chalcopyrite interface has been studied intensively; it was found that, depending on the surface S/Se-content of the chalcopyrite thin-film solar cell absorber, significant intermixing takes place at the interface.[2−4] While we did not find any indications for a significant intermixing at the CdS/kesterite interface in our previous study of the CdS/Cu_2ZnSnS_4 interface,[5] intermixing processes might very well be expected at the CdS/$Cu_2ZnSnSe_4$ (CZTSe) interface. Consequently, we have investigated a sample series based on "Zn-terminated" CZTSe absorbers[6] with CdS buffers of different thicknesses using electron and X-ray spectroscopies of varying surface sensitivity to characterize the chemical structure of this buried interface. On the basis of these insights, we compare the results to our previous findings for the CdS/CIGSe interface in order to identify similarities and differences.

Figure 1 shows the X-ray photoelectron spectroscopy (XPS) survey spectra of the investigated CdS/CZTSe sample series. As expected, all Cd, S, Cu, Zn, Sn, and Se photoemission and Auger lines are present. The Cu, Zn, Sn, and Se peaks decrease in intensity, and the Cd and S peaks increase with increasing CBD time. In addition, rather substantial C-, O-, and Na-related XPS and X-ray-excited Auger electron spectroscopy (XAES) signals can be identified. C and O signals are attributed to a surface contamination layer formed during air-exposure and/or to incorporation during deposition of the absorber and buffer layer. The Na signal, which decreases for thicker CdS layers,

Received: February 20, 2017
Accepted: June 9, 2017
Published: June 14, 2017

DOI: 10.1021/acsenergylett.7b00140
ACS Energy Lett. 2017, 2, 1632−1640

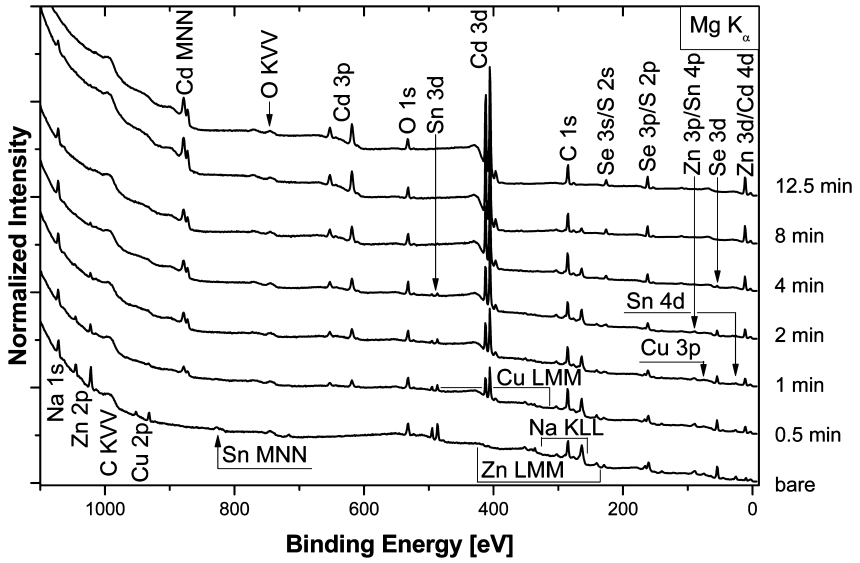

Figure 1. XPS survey spectra (normalized to equal intensity at a binding energy of 600 eV) of the bare CZTSe sample (bottom) and the CdS thickness series (deposition time varied between 0.5 and 12.5 min). All prominent photoemission and Auger lines are labeled. Spectra are vertically offset for clarity.

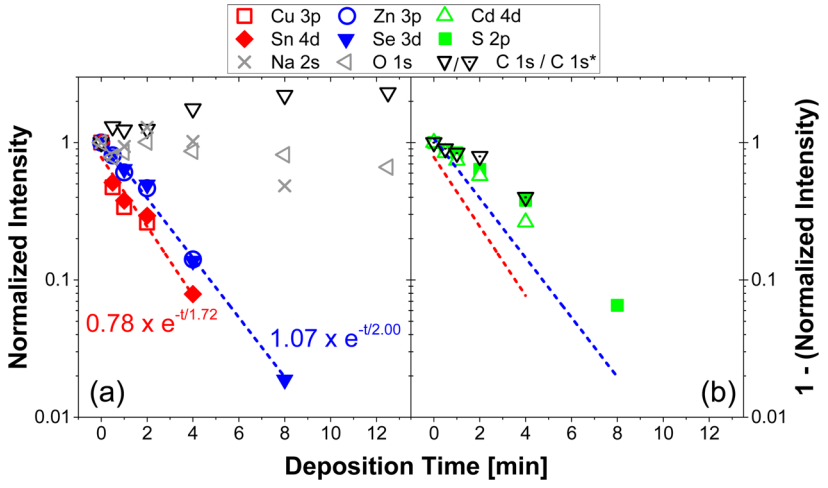

Figure 2. Evolution of the signal intensities of (a) the Cu 3p, Sn 4d, Zn 3p, Se 3d, Na 2s, O 1s, and C 1s and (b) the S 2p, Cd 4d, and C 1s* XPS lines with increasing CdS deposition time shown on a logarithmic scale. Panel b shows the data on a 1 − (Normalized Intensity) scale to allow for a direct comparison with the attenuation behavior shown in panel a. The red and blue dashed lines represent the best $e^{-x/\omega}$ type fits of the Cu 3p and Sn 4d and the Zn 3p and Se 3d signal attenuation. C 1s* is the C 1s intensity corrected by the C 1s signal of the bare absorber.

indicates that sodium diffuses from the soda-lime glass substrate during absorber formation.

In order to evaluate the attenuation behavior of the different core levels independent of analyzer transmission function and inelastic mean free path (IMFP), we make use of the normalized intensities of absorber-related shallow core level signals (Zn 3p, Cu 3p, Na 2s, Se 3d, and Sn 4d) with similar (high) kinetic energies (for Mg Kα: from 1165 eV [Zn 3p] to 1229 eV [Sn 4d]). In addition, the intensities of the C 1s and O 1s lines are also considered. Note that these core levels have higher binding energies and thus lower kinetic energies (971 eV [C 1s] and 826 eV [O 1s]); hence, a higher analyzer transmission and a lower IMFP has to be taken into account for a direct comparison with the intensity evolution of the shallow core levels. Assuming that C and O are exclusively present at the sample surfaces, the impact of different IMFPs is considered to be negligible. The peak intensities were normalized such that the integral intensity of each photoemission line is "one" for the spectrum of the bare absorber surface. With the exception of C and Na, all considered absorber-related photoemission lines decrease with increasing CBD time because of the attenuation by the increasingly thick CdS buffer layer, as shown in Figure 2a. We find that, with increasing deposition time, the Cu 3p and Sn 4d intensities (red symbols) decrease significantly faster than the intensities of the Zn 3p and Se 3d photoemission lines (blue symbols). Note that the intensity evolution in Figure 2a is shown on a logarithmic scale, as it is best suited to show data with an (expected) exponential dependency (see discussion below). To simplify the following analysis, we assume that there is a linear relationship between deposition time and layer thickness; this essentially assumes that the CdS layer grows homogeneously and in a layer-by-layer mode (in reality, of course, the CdS film may not form uniformly on the kesterite surface and possesses a

DOI: 10.1021/acsenergylett.7b00140
ACS Energy Lett. 2017, 2, 1632−1640

detailed nanostructure morphology, and the growth is conducted with an increasing temperature ramp, i.e., under varying thermodynamic conditions, suggesting that the growth at the start might be "slower" than during the end of the deposition process).

As shown in Figure 2a by the dashed red line, the signal attenuation of the Cu 3p and Sn 4d lines was fitted according to the Lambert−Beer law: $I = I_0 \times e^{-t/\omega}$. In this approach, I and I_0 are the attenuated and unattenuated photoemission line intensities, respectively, and ω plays the role of an "attenuation length analogue" in units of deposition time (rather than layer thickness). We find that, employing this model, the Cu 3p and Sn 4d intensity decrease can be best described with ω_1 = 1.72 (±0.20) min, meaning that the 2 min CdS layer will attenuate the Cu 3p and Sn 4d absorber signals to less than $1/e \times I_0$. A similar analysis was performed for the Zn 3p and Se 3d lines (blue data points and dashed blue line in Figure 2a). The best fit is found for ω_2 = 2.00 (±0.20) min, i.e., the "attenuation length" is larger than the one derived for the Cu 3p and Sn 4d lines, and after 2 min, the intensity is reduced to exactly $1/e \times I_0$.

In Figure 2b, the intensity evolution of the buffer-related S 2p and Cd 4d photoemission lines is shown. Again, the considered XPS peaks have a similar (high) kinetic energy (for Mg Kα: 1091 eV [S 2p] and 1242 eV [Cd 4d]). In this case, the line intensities are normalized such that each peak reaches "one" for the thickest buffer layer. They are shown as the difference from one on a logarithmic scale in order to allow a direct comparison to the attenuation behavior of the absorber peaks represented by the corresponding fits for (Cu 3p and Sn 4d) and (Zn 3p and Se 3d) in Figure 2a. The intensity of both buffer-related photoemission lines increases with CBD time, indicated by a decrease on the "1 − (Normalized Intensity)" scale in Figure 2b. For short deposition times (up to 2 min), the S 2p and Cd 4d intensity increase is in accordance with the attenuation of the Zn 3p and Se 3d lines (but not with the Cu 3p and Sn 4d signal evolution), as indicated by the good agreement between the corresponding data points and the blue dashed line (but not the red dashed line) in Figure 2b. In this deposition time regime, the attenuation of the Zn 3p and Se 3d lines ($\propto e^{-t/\omega}$) and the increase of the S 2p and Cd 4d XPS signals ($\propto 1 - e^{-t/\omega}$) can be explained by one value for ω ($\equiv \omega_2$ = 2.00 [± 0.20] min). For longer deposition times, the "1 − (Normalized Intensity)" of the buffer-related photoemission lines exceeds the values expected from the attenuation of the Zn 3p and Se 3d XPS signals. This could be explained by a distinct S and Cd profile in the buffer layer: a lower S and Cd concentration at the *interface* to the absorber and an increasing S and Cd concentration toward the surface of the full buffer layer would lead to such an intensity behavior and be indicative of an intermixed chemical structure in the proximity of the buffer/absorber interface. Note that, qualitatively, these findings are not expected to be influenced by the presence or formation of an inhomogeneous or nonuniform CdS layer. However, the derived ω values represent deposition times that yield "effective" CdS thicknesses to correctly describe the attenuation ($\propto e^{-t/\omega}$) and increase ($\propto 1 - e^{-t/\omega}$) of the absorber and buffer signals, respectively.

In general, we note that this quantification approach is made challenging by the significant presence of sodium, oxygen, and carbon in the form of adsorbates on the surface and/or incorporated in the bulk. As can be seen from the survey spectra in Figure 1 and the data points in Figure 2a, the evolution of the Na, O, and C intensities with CBD time varies, as will be discussed in the following.

The intensity evolution of the Na photoemission line varies from sample to sample, indicating a complex situation. We speculate that at least three different processes may be involved, namely, partial Na removal from the CZTSe surface in the induction period of the CBD CdS process, redeposition during buffer/absorber interface formation, and/or Na diffusion into the buffer layer after CdS deposition. The fact that Na-related XPS peak intensities vary less as a function of CBD time if probed by more bulk-sensitive Al Kα excitation (not shown) points to a distinct Na profile in the upper sample region with an accumulation at the buffer surface. This is in agreement with our observations of other CBD CdS buffers with Na signal (unpublished). However, Na incorporation into the bulk of the buffer layer can also not be excluded. In contrast, we find a mainly constant O 1s and a steadily increasing C 1s line intensity with CBD time. While a constant oxygen intensity points to surface adsorption during sample handling, the increasing carbon intensity suggests a (partial) incorporation into the buffer layer. The latter is supported by the fact that C 1s* (CBD time) = C 1s (CBD time) − C 1s (0 min) in Figure 2b agrees well with the evolution of the S 2p and Cd 4d intensities.

Overall, the fact that the S 2p, Cd 4d, Zn 3p, and Se 3d intensity behaviors all can be described by "attenuation length analogues" that are larger than that of Cu 3p and Sn 4d suggests a "redistribution" of the former elements at the CdS/CZTSe interface. The simplest explanation is a CBD-induced formation of a Zn−Se−Cd−S intermixed buffer/absorber interface, as will be discussed below.

Note that previous Raman spectroscopy and scanning electron microscopy analyses of similarly prepared Zn-terminated CZTSe samples indicate the presence of some ZnSe on the surface and in the bulk of respective kesterite absorber layers.[7] Hence, another scenario that could (to some extent) explain the different attenuation is the coexistence of ZnSe and CdS and a preferential growth of CdS on the absorber. However, we will present arguments below that indicate that this scenario is less likely.

To determine an approximate surface composition of the CZTSe absorber, we use the Zn 3p, Cu 3p, Se 3d, and Sn 4d line intensities and assume that the observed Na, C, and O contributions are exclusively accumulated at the outer CZTSe surface (i.e., not incorporated into the absorber or located at inner surfaces such as grain boundaries). In this case, one can determine a "partial" surface composition, because the attenuation of the absorber lines (at comparable kinetic energies) will be similar for all elements; the result is "$Cu_{1.4}Zn_{2.6}Sn_{1.0}Se_{3.9}$". We estimate the uncertainty for this quantification to be at least 20%, in particular because of the uncertainty in photoionization cross section and the assumptions made above. The error bar for the Zn content is likely to be even larger, as the Zn 3p is partially superimposed on the broad and indistinct Sn 4p line, which makes it challenging to determine the area accurately.

The thus-derived partial surface composition ($Cu_{1.4}Zn_{2.6}Sn_{1.0}Se_{3.9}$) significantly deviates from a stoichiometric $Cu_2ZnSnSe_4$ kesterite in relative Cu and Zn content. Furthermore, in comparison to the bulk composition of $Cu_{1.9}Zn_{1.4}Sn_{1.0}Se_{4.0}$ (see Experimental Methods), we find a particularly Zn-rich surface, in agreement with the Zn-rich

DOI: 10.1021/acsenergylett.7b00140
ACS Energy Lett. 2017, 2, 1632−1640

"termination"[6] and the previously suggested presence of ZnSe at the absorber surface.[7]

To further characterize the chemical structure of the interfacial layer formed at the buried CdS/CZTSe interface and to compare it with the interface structure of CdS/CIGSe samples, we also investigated the CdS/CZTSe sample series by S $L_{2,3}$/Se $M_{2,3}$ X-ray emission spectroscopy (XES). Figure 3

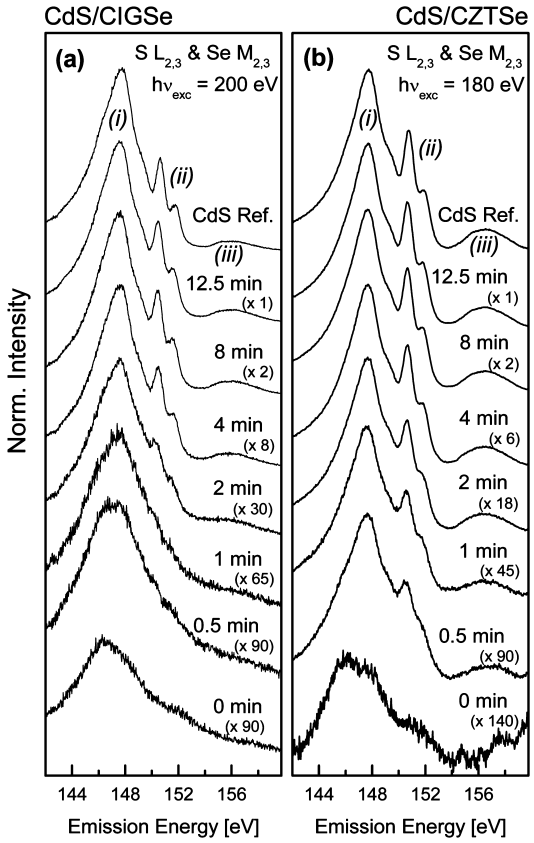

Figure 3. S $L_{2,3}$/Se $M_{2,3}$ XES spectra of (a) a CdS/CIGSe thickness series (modified from ref 4; copyright 2010 American Institute of Physics) compared to (b) the spectra of the CdS/CZTSe thickness series. The main features are labeled (*i*)−(*iii*). Spectra are normalized to equal peak height above background and vertically offset for clarity. Note the different magnification factors.

compares the XES data of the CdS/CZTSe sample series (right panel (b), excited at $h\nu$ = 180 eV) with that of a previously measured CdS/CIGSe sample series (left panel (a), excited at $h\nu$ = 200 eV; modified from ref 4). Note that, for both series, the *same* CBD process was used to deposit the CdS layer. As expected, the sulfur signal intensity increases with CBD time (i.e., with CdS thickness; note the different magnification factors). For the bare absorbers, the spectra show the Se $M_{2,3}$ emission, which is much weaker (by approximately 2 orders of magnitude) than the S $L_{2,3}$ emission, primarily because of a lower fluorescence yield. For the bare CZTSe spectrum, additional (weak) spectral intensity above 154 eV is assigned to Sn-related emissions (in particular Sn M_2N_1 at 619 eV and Sn M_5 at 483 eV[8]), excited by higher harmonics of the undulator and detected in higher orders of the spectrometer. Also, the tail of the elastically scattered (Rayleigh) line influences the background shape in this region (note the lower excitation energy for the CZTSe series).

Following ref 9, the prominent S $L_{2,3}$ spectral features are associated with (i) S 3s states, (ii) Cd 4d-derived bands, and (iii) the upper valence band, all of them decaying into S 2p core holes. For the CdS/CIGSe samples, the presence of a S-containing interlayer between CdS and the CIGSe absorber, most likely in the form of $(In_{1-x}Ga_x)_yS_z$, was concluded from the evolution of the S $L_{2,3}$/Se $M_{2,3}$ emission,[2,4] mainly based on the fact that the S $L_{2,3}$ emission intensity increased with CdS deposition time but did not show the distinct Cd 4d-derived features (ii) at the growth start. In contrast, for the CdS/CZTSe samples (in particular the 0.5 min CdS/CZTSe sample), pronounced Cd 4d-derived emission features can be observed, indicating a significantly decreased induction period of the CBD-CdS deposition on the CZTSe absorber. Directly comparing the S $L_{2,3}$ emission of the 0.5 min CdS/CZTSe with that of the 12.5 min sample (Figure 4) reveals, however, that

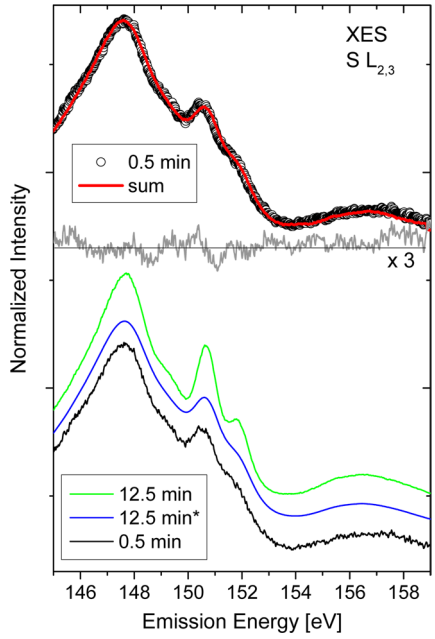

Figure 4. Bottom: Area-normalized S $L_{2,3}$ XES spectra of the 0.5 min (black line) and 12.5 min (green line) CdS/CZTSe sample compared to the Lorentzian-broadened 12.5 min spectrum (blue line, "12.5 min*"). Top: Direct comparison of the S $L_{2,3}$ XES spectrum of the 0.5 min (open circles) CdS/CZTSe sample with the spectral "sum" (red line) of 0.94 × the Lorentzian-broadened 12.5 min spectrum (12.5 min*) + 0.55 × the spectrum of the bare CZTSe absorber (from Figure 3b). The magnified residuum (difference between data and fit) is shown for comparison.

the Cd 4d-derived features are much less distinct (i.e., broader) at the growth start. Indeed, if the 12.5 min spectrum is broadened with a Lorentzian of suitable width (fwhm = 1.7 eV → "12.5 min*" spectrum in Figure 4), the Cd 4d-derived features (ii) resemble those of the 0.5 min spectrum. The sum spectrum in Figure 4 represents a superposition of the broadened 12.5 min* spectrum (×0.94) and the spectrum of the bare CZTSe sample (×0.55). The agreement with the 0.5 min spectrum is very good, indicating that the sulfur deposited during the early stages of the CBD-CdS deposition is mainly present in a CdS-type environment; the broadening is probably due to a poorly defined physical structure (i.e., different bond lengths and angles) at the interface. Furthermore, we note that these features are derived from complex band structures (rather

DOI: 10.1021/acsenergylett.7b00140
ACS Energy Lett. 2017, 2, 1632−1640

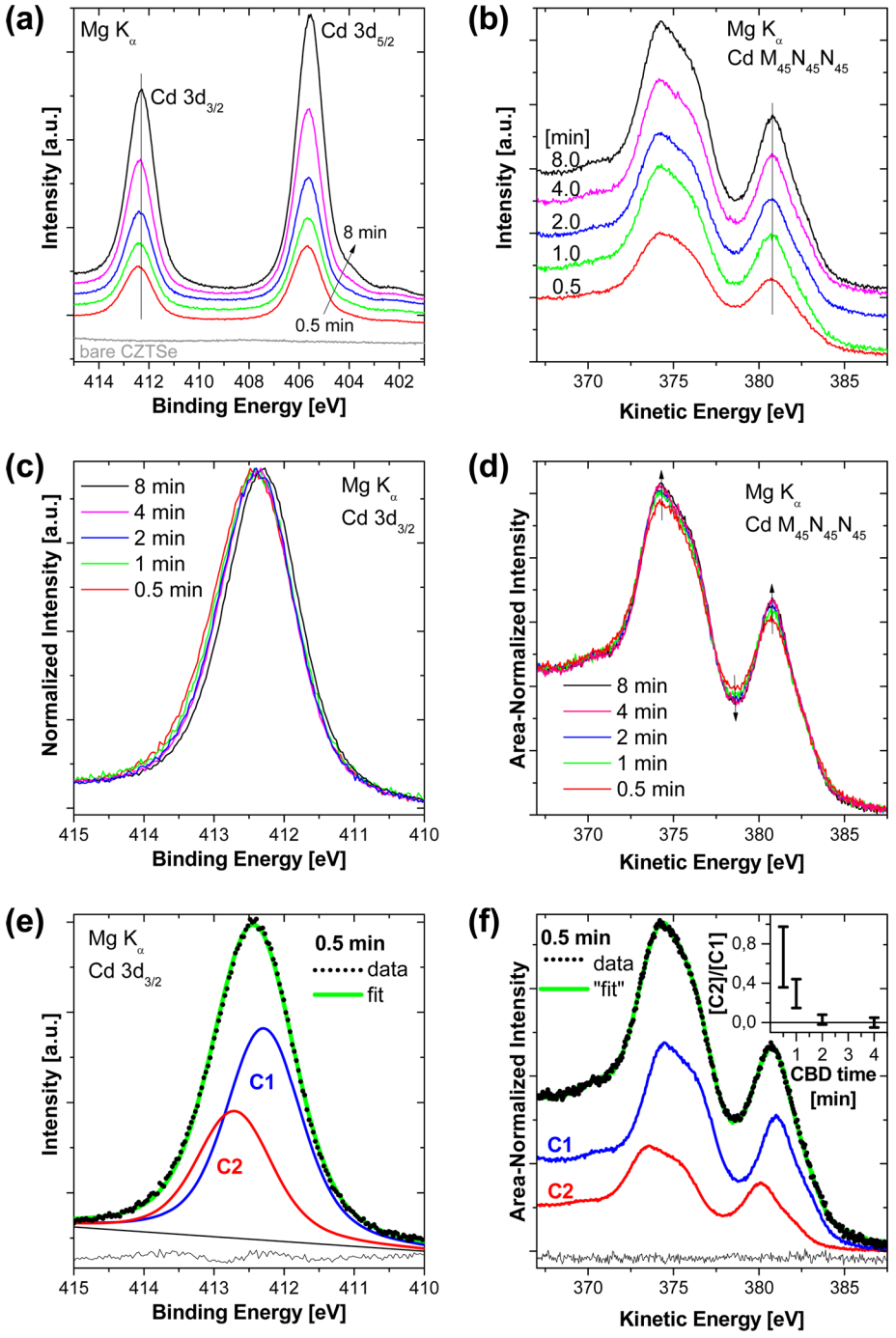

Figure 5. Evolution of the Cd 3d XPS (a) and the Cd $M_{45}N_{45}N_{45}$ XAES (b) spectra with increasing CBD-CdS deposition time. Panels c and d show the same, but background-corrected and maximum-normalized, spectra to emphasize spectral differences. Panels e and f show the representation of the broadest spectra (0.5 min CdS/CZTSe sample) as the sum of two components (C1 and C2, see text for fitting details). The inset in panel f shows that the C2/C1 intensity ratio decreases with increasing CdS deposition time.

than core-to-core fluorescence transitions); thus, a simple "CdS-like" picture cannot be sufficient for a perfect description of the electronic structure at the CdS/CZTSe interface for very thin CdS layers, leading to some statistically relevant deviations in the residual.

The formation of S−Cd bonds right from the start of the CBD process is different from the growth start of the CdS/CIGSe interface. In that system, the CBD process includes an induction period of approximately 2 min, i.e., no significant deposition of "true" CdS is taking place during that time (see, e.g., the fact that features (ii) in Figure 3a are missing for deposition times shorter than 2 min).

One explanation for this different growth start behavior could be an ion-exchange mediated by the complexes formed in the chemical bath.[10,11] In a first approximation, we use ZnSe as a model compound to represent the Zn-terminated CZTSe surface. This is justified by previous Raman spectroscopy and scanning electron microscopy analysis results of similarly prepared samples that suggest the presence of ZnSe on the kesterite surface.[7] However, also note that no thermodynamic

DOI: 10.1021/acsenergylett.7b00140
ACS Energy Lett. 2017, 2, 1632−1640

data such as, e.g., the solubility product for CZTSe, is known. $[Cd(NH_3)_4]^{2+}$ is the dominant Cd-species in the CdS CBD ambience. Likewise, for Zn, the tetra-ammine complex $[Zn(NH_3)_4]^{2+}$ is favored in an aqueous ammonia environment. Consequently, before significant CdS deposition starts, the chemical processes in the CBD solution at the absorber surface can be described by eq 1:

$$ZnSe + [Cd(NH_3)_4]^{2+} \leftrightarrow CdSe + [Zn(NH_3)_4]^{2+} \quad (1)$$

According to Le Chatelier's principle, the equilibrium of reaction 1 will, at growth start, be driven to the right-hand side because, in terms of concentration, [ZnSe] ≫ [CdSe] and $[[Cd(NH_3)_4]^{2+}] \gg [[Zn(NH_3)_4]^{2+}]$. Hence, in the initial stages of a CdS CBD process, the formation of Cd−Se bonds at the expense of Zn−Se bonds (present at the CZTSe surface) is thermodynamically preferred. Moreover, the solubilities of ZnSe and CdSe, as well as the stability constants of the respective complexes, support this picture. For ZnSe and CdSe, K_{sp} values range from 1.0×10^{-31} to 4.7×10^{-27} and from 5.0×10^{-35} to 1.1×10^{-33}, respectively.[12] The stability constants of the complexes are $\beta^{Cd^{2+}}_{NH_3,4} = 1.2 \times 10^7$ and $\beta^{Zn^{2+}}_{NH_3,4} = 4.0 \times 10^9$.[13,14] The analysis of the solubilities and stability constants reveals that CdSe is significantly less soluble than ZnSe, while $[Zn(NH_3)_4]^{2+}$ is clearly more stable than $[Cd(NH_3)_4]^{2+}$. These points also support the conclusion that the equilibrium of reaction 1 is on the side of CdSe and $[Zn(NH_3)_4]^{2+}$ at the growth start. We thus argue that the induction period for the CdS growth start on CZTSe is rather short, given that the nucleation centers necessary for CdS growth could be formed rather quickly. Another reason for the shortened induction period could be an enhanced ion-exchange mediated decomposition of the thiourea in the chemical bath; a similar catalytic effect, the hydroxide-mediated catalysis of thiourea decomposition,[15] is well-known to expedite film formation in the chemical bath.

In order to understand the difference to the CdS/CIGSe system, we—in a first approximation—use In_2Se_3 as a model compound to represent the generally Cu-poor CIGSe surface (note that no thermodynamic data such as, for example, the solubility product for CIGSe, is known). In analogy to the approach above, the solubilities of In_2Se_3 and CdSe, together with stability constants of the dominant cadmium and indium complexes in aqueous ammonia, are compared next. To compare the solubilities, one has to consider a range of 2.3×10^{-19} to 5.2×10^{-19} for In_2Se_3 and 7.1×10^{-18} to 3.3×10^{-17} for CdSe (see ref 12 for more details). Hence, In_2Se_3 is less soluble than CdSe. Together with the fact that indium does not form stable complex compounds in aqueous ammonia,[16] this strongly suggests that there is no complex-mediated formation of Cd−Se bonds at the expense of In−Se bonds for the CdS/CIGSe system.

In order to check whether our XPS and XAES data support the model of Cd−Se bond formation at the growth start, we consult the corresponding Cd-related photoemission and Auger lines. Figure 5 shows the evolution of the Cd 3d (a) and $M_{45}N_{45}N_{45}$ (b) spectra with increasing CBD-CdS deposition time (0 to 8 min); as expected, the Cd-related signals increase in intensity. The peak-height-normalized and background-corrected Cd $3d_{3/2}$ (c) and $M_{45}N_{45}N_{45}$ (d) spectra reveal a significant broadening for short deposition times, indicating the presence of more than one Cd species. The spectra of the 8 min CdS/CZTSe sample (i.e., the thickest CdS film in this spectral series) are the narrowest, both for the Auger and XPS lines. Assuming that they are representative for one single Cd species, we use them in the following to fit the spectra of the samples prepared using shorter CBD deposition times. As shown for the 0.5 min CdS/CZTSe sample in Figure 5e,f, the spectra can indeed be represented by the sum of two components. In the case of the Cd $M_{45}N_{45}N_{45}$ spectra, the best agreement is reached with two 8 min CdS/CZTSe Cd $M_{45}N_{45}N_{45}$ spectra, "C1" and "C2", shifted by 0.9 eV. Using two Voigt functions (of the same width) with a set intensity ratio of C1/C2 and employing a linear background, also the Cd $3d_{3/2}$ XPS spectrum in Figure 5e can be represented by a sum of two contributions. Note that, although a broadening of the Cd 3d line can clearly be observed (Figure 5c), the chemical shift of the Cd 3d line for different Cd species is too small for the energy resolution of the present XPS data to allow for an unambiguous free fit (i.e., without a fixed intensity ratio). Nevertheless, analyzing the Auger spectra of the 1, 2, and 4 min CdS/CZTSe samples, we find that the C2/C1 intensity ratio significantly decreases with increasing CdS deposition time (see inset in Figure 5f). This is in agreement with the observation that the Cd 3d and Cd $M_{45}N_{45}N_{45}$ line widths decrease with increasing CdS deposition time. As a result, we identify C2 as a Cd species that is present in the proximity of the CdS/CZTSe interface, while C1 represents Cd in a CdS (-like) environment.

The modified Auger parameter (α') of cadmium, which we compute from the sum of the binding energy (E_B) of the Cd $3d_{3/2}$ photoemission line and the kinetic energy (E_K) of the Cd $M_4N_{45}N_{45}$ Auger line, is shown in Figure 6. Note that we use the Cd $3d_{3/2}$ line from Figure 5c (and not the more intense $3d_{5/2}$ XPS peak) to avoid the Mg $K\alpha_{3,4}$-excited $3d_{3/2}$ satellite lines that overlap with the $3d_{5/2}$ peak. In order to make a comparison with α' literature values [which are mainly based

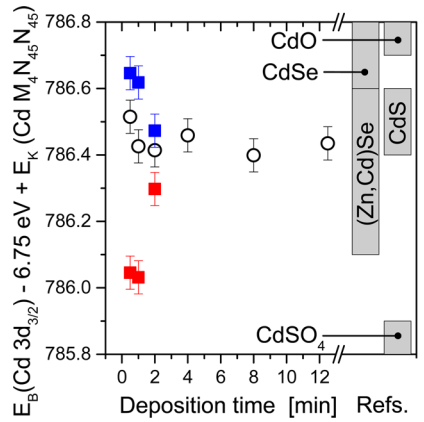

Figure 6. Evolution of the modified Auger parameter (α') of Cd [i.e., the sum of the binding energy (E_B) of the Cd $3d_{3/2}$ photoemission line and the kinetic energy (E_K) of the Cd $M_4N_{45}N_{45}$ Auger line] with increasing CBD CdS deposition time (black open symbols). For short deposition times, the Cd 3d and Cd MNN spectra in Figure 5 indicate the presence of more than one species. Decomposition into two contributions results in two α' sets in the early stages of the CBD deposition. They are shown as blue and red solid symbols and refer to species C1 and C2, respectively, as indicated in Figure 5e,f. For comparison, reference positions for CdS, CdSe, and (Zn,Cd)Se compounds from refs 17−19 are indicated. The indicated error bars are dominated by the uncertainty in the determination of the energy position of the individual components.

DOI: 10.1021/acsenergylett.7b00140
ACS Energy Lett. 2017, 2, 1632−1640

on E_B(Cd $3d_{5/2}$)], we subtract the $3d_{5/2} - 3d_{3/2}$ doublet separation of 6.75 eV (mean value of the doublet separation values in ref 16) from our sum to derive the α' values. For the Auger line, we (for now) assume a single species and employ the peak maximum as seen in Figure 5d. The thus-derived α' values are shown as a function of CBD deposition time in Figure 6 (open black circles), together with α' ranges for CdSe, CdS, (Zn,Cd)Se, CdO, and $CdSO_4$ (gray boxes) reported in the literature.[17−19] For $Cd(OH)_2$, one finds α' values between 784.9 and 785.1 eV,[17] which is outside of the α' range in Figure 6 and thus excluded in our analysis. Within the experimental uncertainty, the determined values are in agreement with the formation of CdS or (Zn,Cd)Se for all CBD deposition times. The computed α' values for the two species formed in the early stages of the CBD deposition (i.e., C1 and C2, as discussed above) are shown as blue (C1) and red (C2) solid squares in Figure 6. Taking the experimental uncertainty into account, the α' values of C1 are in agreement with the formation of Cd−Se and/or Cd−S bonds, whereas the α' values of C2 point to the formation of Cd−Se−Zn bonds. The presence of CdO (→ C1) or $CdSO_4$ (→ C2) seems also possible (taking the uncertainty of the reference data into account). However, the latter can likely be excluded because no spectral fingerprint for sulfate was observed in the S 2p XPS and $L_{2,3}$ XES spectra. Considering that no major Zn 3p and Se 3d line intensities can be observed for deposition times of 4 min or more (see Figure 2a), the derived "single-species" α' values are concluded to be indicative for the formation of CdS.

With evidence for the formation of Cd−Se−Zn bonds and the reasoning for a Zn−Cd ion exchange in the chemical bath, the scenario of a preferential growth of CdS on CZTSe compared to that on a ZnSe surface phase as an explanation for the different attenuation behavior (see Figure 2) appears to be rather unlikely. We rather argue that with the finding of an interfacial region with Cd−S,Se and Cd−Se−Zn bonds, the XPS and XAES results are best explained by an intermixed Cd(S,Se)−(Zn,Cd)Se material formed in the proximity of the CdS/CZTSe interface. This is most likely a result of an incomplete ion exchange according to eq 1, a redeposition or incorporation of Zn in the formed CdSe, and/or the initial interfacial bond formation during the growth start. A schematic presentation of the suggested CdS/CZTSe interface structure is depicted in Figure 7. Future studies of the interface between CBD-CdS and stoichiometric (i.e., not Zn-terminated) CZTSe surfaces have to show whether this interlayer generally forms at the CdS/CZTSe interface or whether it is a peculiarity of the Zn-terminated CZTSe absorber that exhibits a ZnSe surface layer.[7]

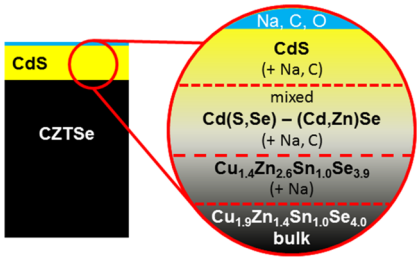

Figure 7. Schematic presentation of the chemical structure of the CdS/CZTSe interface. Adsorbates at the outermost surface are indicated in blue.

A combination of electron and X-ray spectroscopies was used to investigate the chemical structure of the CdS/$Cu_2ZnSnSe_4$ (CZTSe) interface. We find a "redistribution" of Zn, Se, Cd, and S in the proximity of the CdS/CZTSe interface during interface formation in the chemical bath, which represents a significantly different situation as compared to our previous study of the CdS/Cu_2ZnSnS_4 interface.[5] The evolution of the shallow core level intensities with increasing CdS deposition time (and thus CdS thickness) suggests that a Zn−Se−Cd−S interlayer forms between the CdS buffer and the CZTSe absorber. We find evidence for the presence of Cd−S,Se and Cd−Se−Zn bonds at the buffer/absorber interface. As a result, we propose the formation of an interfacial region that has a mixed Cd(S,Se)−(Cd,Zn)Se character. As a potential underlying chemical mechanism, we suggest an ion exchange mediated by the amine complexes present in the chemical bath, which most likely also changes the compound formation kinetics and thus would explain the significantly reduced induction period. This buffer/absorber formation process and structure is markedly different from that of the widely studied CdS/Cu(In,Ga)Se_2 interface.[4] This finding emphasizes that it is advisible to thoroughly characterize the specific heterostructure under consideration instead of basing optimization efforts on models derived for a seemingly related, but in detail very different, system. This might be one cornerstone to overcome current performance limitations.

EXPERIMENTAL METHODS

CZTSe thin-film solar cell absorbers of approximately 1.4 μm thickness prepared within one deposition run were grown by four-source thermal coevaporation on Mo/glass substrates at National Renewable Energy Laboratory (NREL; for more details, see ref 6). During sample cooling, a reduced but nonzero Zn rate was applied, which results in a Zn-rich absorber surface "termination".[6] By bulk-sensitive X-ray fluorescence analysis, an average composition of Zn/Sn = 1.4 and Cu/(Zn+Sn) = 0.8 was determined. Previous Raman spectroscopy and scanning electron microscopy analysis of similarly prepared samples indicates the presence of some ZnSe on the surface and in the bulk of respective kesterite absorber layers.[7] Nevertheless, solar cell devices based on these CZTSe absorbers have achieved power conversion efficiencies up to 9.8%.[20] For the present study, the CdS layer thickness was varied by interrupting the chemical bath deposition after 0.5, 1, 2, 4, 8, and 12.5 min. For the standard deposition time (12.5 min), the thickness of the CdS layer is approximately 50 nm, as determined by the optical method described in ref 21. After preparation, the CdS/CZTSe structures were sealed under inert gas and sent from NREL to Helmholtz-Zentrum Berlin für Materialien und Energie GmbH (HZB) and Advanced Light Source (ALS) for characterization. At HZB, the samples were unpacked and mounted in a N_2-purged glovebox and transferred directly into the connected ultrahigh vacuum (UHV) surface analysis system (base pressure in the analysis chamber: $< 5 \times 10^{-10}$ mbar). The chemical surface/interface structure of the CdS/CZTSe samples was investigated by XPS as well as XAES. Mg/Al Kα excitation (SPECS XR 50 twin-anode X-ray source) and a Specs Phoibos 150 MCD-9 electron analyzer were used. The latter was calibrated according to ref 17. Pass energies (and step sizes) of 50 (1), 30 (0.05), and 20 (0.03) eV with dwell times of 0.1 s/point were used for collecting the XPS survey, the XAES, and the XPS detail spectra, respectively. No charge compensation was applied. The

DOI: 10.1021/acsenergylett.7b00140
ACS Energy Lett. 2017, 2, 1632−1640

XPS line intensities were quantified (if not specified differently) by fitting them with Voigt profiles and a linear background using the curve-fitting and data analysis program *FITYK* (version 0.9.8).[22] The core level spectra of the whole sample set were fitted simultaneously with coupled widths for all Gaussian and Lorentzian contributions. For spin−orbit split spectra, the intensities of the doublet peaks were set according to the respective multiplicity ($2j + 1$). Note that the Zn 3p core level is partially superimposed with the broad and indistinct Sn 4p line, which is challenging to account for in the fit procedure. Thus, the uncertainty in the quantification of the Zn 3p line is expected to be larger compared to that of other core levels. Because only photoemission lines with similar kinetic energies are considered for quantitative analysis, the analyzer transmission function and the IMFP are assumed to be identical, allowing elemental ratios and/or surface compositions to be calculated based on only the fit-derived intensities and tabulated photoionization cross sections.[23,24] Note that the 12.5 min sample showed a small charging shift of <0.2 eV in XPS. While such a small shift still allows a quantitative analysis of the peak area, we will refrain from using this sample for our peak shift analysis, with the exception of the modified Auger parameter, which is independent of charging-related energy shifts.

At the ALS, the samples were briefly exposed to air while being mounted on the sample holder before transfer into the UHV analysis chamber ($<5 \times 10^{-8}$ mbar) of the SALSA endstation[25] at Beamline 8.0.2. For XES measurements, which are characterized by a significantly longer attenuation length compared to the IMFP of XPS and XAES, we used a high-transmission, high-resolution soft X-ray spectrometer;[26] an excitation energy of 180 eV; and a spectral resolving power at the S $L_{2,3}$ edge of $E/\Delta E \approx 1000-1200$. The energy scale of the S $L_{2,3}$ XES spectra was calibrated using a CdS reference.[27]

AUTHOR INFORMATION

Corresponding Author

*E-mail: marcus.baer@helmholtz-berlin.de.

ORCID

Marcus Bär: 0000-0001-8581-0691

Notes

The authors declare no competing financial interest.

ACKNOWLEDGMENTS

M.B. and R.G.W. are grateful to the Impuls- und Vernetzungsfonds of the Helmholtz Association (VH-NG-423) and to the European Union's Horizon 2020 research and innovation program (Grant Agreement No. 640868) for partial funding. The ALS is supported by the Office of Basic Energy Sciences of the U.S. Department of Energy under Contract No. DE-AC02-05CH11231.

REFERENCES

(1) Todorov, T. K.; Tang, J.; Bag, S.; Gunawan, O.; Gokmen, T.; Zhu, Y.; Mitzi, D. B. Beyond 11% Efficiency: Characteristics of State-of-the-Art $Cu_2ZnSn(S,Se)_4$ Solar Cells. *Adv. Energy Mater.* **2013**, *3*, 34−38.

(2) Heske, C.; Eich, D.; Fink, R.; Umbach, E.; van Buuren, T.; Bostedt, C.; Terminello, L. J.; Kakar, S.; Grush, M. M.; Callcott, T. A.; et al. Observation of intermixing at the buried CdS/Cu(In, Ga)Se_2 thin film solar cell heterojunction. *Appl. Phys. Lett.* **1999**, *74*, 1451−1453.

(3) Weinhardt, L.; Bär, M.; Pookpanratana, S.; Morkel, M.; Niesen, T. P.; Karg, F.; Ramanathan, K.; Contreras, M. A.; Noufi, R.; Umbach, E.; et al. Sulfur gradient-driven Se diffusion at the CdS/CuIn$(S,Se)_2$ solar cell interface. *Appl. Phys. Lett.* **2010**, *96*, 182102.

(4) Pookpanratana, S.; Repins, I.; Bär, M.; Weinhardt, L.; Zhang, Y.; Félix, R.; Blum, M.; Yang, W.; Heske, C. CdS/Cu(In,Ga)Se_2 interface formation in high-efficiency thin film solar cells. *Appl. Phys. Lett.* **2010**, *97*, 074101.

(5) Bär, M.; Schubert, B.-A.; Marsen, B.; Wilks, R. G.; Pookpanratana, S.; Blum, M.; Krause, S.; Unold, T.; Yang, W.; Weinhardt, L.; et al. Cliff-like conduction band offset and KCN-induced recombination barrier enhancement at the CdS/Cu_2ZnSnS_4 thin-film solar cell heterojunction. *Appl. Phys. Lett.* **2011**, *99*, 222105.

(6) Repins, I.; Beall, C.; Vora, N.; DeHart, C.; Kuciauskas, D.; Dippo, P.; To, B.; Mann, J.; Hsu, W.-C.; Goodrich, A.; et al. Co-evaporated $Cu_2ZnSnSe_4$ films and devices. *Sol. Energy Mater. Sol. Cells* **2012**, *101*, 154−159.

(7) Vora, N.; Blackburn, J.; Repins, I.; Beall, C.; To, B.; Pankow, J.; Teeter, G.; Young, M.; Noufi, R. Phase identification and control of thin films deposited by co-evaporation of elemental Cu, Zn, Sn, and Se. *J. Vac. Sci. Technol., A* **2012**, *30*, 051201.

(8) Bearden, J. A. X-Ray Wavelengths. *Rev. Mod. Phys.* **1967**, *39*, 78−124.

(9) Meisel, A.; Leonhardt, G.; Szargan, R. *X-Ray Spectra and Chemical Binding*; Springer Series in Chemical Physics; Springer: Berlin, 1989; Vol. *37*.

(10) Ortega-Borges, R.; Lincot, D. Mechanism of Chemical Bath Deposition of Cadmium Sulfide Thin Films in the Ammonia-Thiourea System − In Situ Kinetic Study and Modelization. *J. Electrochem. Soc.* **1993**, *140*, 3464−3473.

(11) Bär, M.; Weinhardt, L.; Heske, C.; Muffler, H.-J.; Lux-Steiner, M. Ch.; Umbach, E.; Fischer, Ch.-H. Cd^{2+}/NH_3-treatment of Cu(In,Ga)$(S,Se)_2$ thin film solar cell absorbers − a model for the performance-enhancing processes in the partial electrolyte. *Prog. Photovoltaics* **2005**, *13*, 571−577.

(12) As the formal valency of Zn in ZnSe and Cd in CdSe is the same, we can directly compare the solubility products taken from http://www.novedu.ru/anotes/refer/ctpr.htm. In contrast, in order to be able to compare the solubility of In_2Se_3 and CdSe, the valency must be taken into account based on the corresponding dissociation reactions ($In_2Se_3 \leftrightarrow 2In^{3+} + 3Se^{2-}$ and $CdSe \leftrightarrow Cd^{2+} + Se^{2-}$). According to these reactions, the solubility products can be written as $K_{SP}^{In_2Se_3} = [In^{3+}]^2 \times [Se^{2-}]^3 = [In^{3+}]^2 \times [3/2 \times In^{3+}]^3 = 1.0 \times 10^{-93} - 5.6 \times 10^{-92}$ and $K_{SP}^{CdSe} = [Cd^{2+}] \times [Se^{2-}] = 5.0 \times 10^{-35} - 1.1 \times 10^{-33}$ (taken from the website stated above). Thus, one has to compare $[In^{3+}] = \sqrt[5]{\frac{2}{3} K_{SP}^{In_2Se_3}} = 2.3 \times 10^{-19} - 5.2 \times 10^{-19}$ with $[Cd^{2+}] = \sqrt{K_{SP}^{CdSe}} = 7.1 \times 10^{-18} - 3.3 \times 10^{-17}$. Note, however, that we compare here the metal ion concentrations in a saturated *aqueous salt* solution; for *ammonia-containing* solutions, the respective solubilities may differ but are not available in the literature.

(13) *Holleman-Wiberg's Inorganic Chemistry*; Wiberg, N., Ed.; Academic Press: New York, 2001.

(14) To compare the $[Cd(NH_3)_4]^{2+}$ and $[Zn(NH_3)_4]^{2+}$ formation according to eq 1, the influence of $[NH_3]^n$ can be neglected, because at the beginning of the CBD process, $[NH_3]$ is large and close to 1 mol/L.

(15) Hodes, G. *Chemical Solution Deposition of Semiconductor Films*; Marcel Dekker Inc.: New York, 2003.

(16) Busev, A. I. *The Analytical Chemistry of Indium*; Pergamon Press: Oxford, London, New York, Paris, 1962; p 34.

(17) Werner, W. S. M.; Smekal, W.; Powell, C. J. *NIST Database for the Simulation of Electron Spectra for Surface Analysis*, Version 1.1; National Institute of Standards and Technology: Gaithersburg, MD, 2014.

(18) Briggs, D.; Seah, M. P. *Auger and X-Ray Photoelectron Spectroscopy: Practical Surface Analysis*; Wiley: New York, 1990; Vol. *1*, appendix 1.

DOI: 10.1021/acsenergylett.7b00140
ACS Energy Lett. 2017, 2, 1632−1640

(19) Moulder, J. F.; Stickle, W. F.; Sobol, P. E.; Bomben, K. D. *Handbook of X-ray Photoelectron Spectroscopy*; Perkin-Elmer Corporation, Physical Electronics Division: Eden Prairie, MN, 1992; Apendix A: Auger Parameters.
(20) Repins, I. L.; Li, J. V.; Kanevce, A.; Perkins, C. L.; Steirer, K. X.; Pankow, J.; Teeter, G.; Kuciauskas, D.; Beall, C.; Dehart, C.; et al. Effects of deposition termination on $Cu_2ZnSnSe_4$ device characteristics. *Thin Solid Films* **2015**, *582*, 184−187.
(21) Mann, J. R.; Vora, N.; Repins, I. L. In-situ thickness measurements of chemical bath-deposited CdS. *Sol. Energy Mater. Sol. Cells* **2010**, *94*, 333−337.
(22) FITYK 0.9.8 code: Wojdyr, M. FITYK: A general-purpose peak fitting program. *J. Appl. Crystallogr.* **2010**, *43*, 1126−1128.
(23) Yeh, J. J.; Lindau, I. Atomic subshell photoionization cross sections and asymmetry parameters: $1 \leqslant Z \leqslant 103$. *At. Data Nucl. Data Tables* **1985**, *32*, 1−55.
(24) Scofield, J. H. Hartree-Slater Subshell Photoionization Cross-Sections at 1254 and 1487 eV. *J. Electron Spectrosc. Relat. Phenom.* **1976**, *8*, 129−137.
(25) Blum, M.; Weinhardt, L.; Fuchs, O.; Bär, M.; Zhang, Y.; Weigand, M.; Krause, S.; Pookpanratana, S.; Hofmann, T.; Yang, W.; et al. Solid and liquid spectroscopic analysis (SALSA) − a soft x-ray spectroscopy endstation with a novel flow-through liquid cell. *Rev. Sci. Instrum.* **2009**, *80*, 123102.
(26) Fuchs, O.; Weinhardt, L.; Blum, M.; Weigand, M.; Umbach, E.; Bär, M.; Heske, C.; Denlinger, J.; Chuang, Y.-D.; McKinney, W.; et al. High-resolution, high-transmission soft x-ray spectrometer for the study of biological samples. *Rev. Sci. Instrum.* **2009**, *80*, 063103.
(27) Weinhardt, L.; Fuchs, O.; Fleszar, A.; Bär, M.; Blum, M.; Weigand, M.; Denlinger, J. D.; Yang, W.; Hanke, W.; Umbach, E.; et al. Resonant inelastic soft x-ray scattering of CdS: A two-dimensional electronic structure map approach. *Phys. Rev. B: Condens. Matter Mater. Phys.* **2009**, *79*, 165305.

DOI: 10.1021/acsenergylett.7b00140
ACS Energy Lett. 2017, 2, 1632−1640